IAHR AIRH
Taylor & Francis
Taylor & Francis Group

Journal of Hydraulic Research Vol. 50, No. 2 (2012), pp. 171–180
http://dx.doi.org/10.1080/00221686.2012.654668
© 2012 International Association for Hydro-Environment Engineering and Research

Research paper

Local scour at bridge abutments in cohesive soil

MOKHLES M. ABOU-SEIDA, Professor, *Irrigation and Hydraulics Department, Faculty of Engineering, Cairo University, Elorman, Cairo, Egypt.*
Email: mokhlesas@gmail.com

GAMAL H. ELSAEED (IAHR Member), Professor, *Civil Engineering Department, Faculty of Engineering (Shobra), Banha University, 108 Shobra Street, Cairo 11625, Egypt.*
Email: gelsaeed@feng.bu.edu.eg (author for correspondence)

TAREK M. MOSTAFA, Assistant Professor, *Irrigation and Hydraulics Department, Faculty of Engineering, Cairo University, Cairo, Egypt.*
Email: tmsalahe2002@yahoo.com

ELZAHRY F. ELZAHRY, PhD Candidate, *Civil Engineering Department, Faculty of Engineering (Shobra), Banha University, 108 Shobra Street, Cairo 11625, Egypt.*
Email: elzahry@hotmail.com

ABSTRACT
The results of a laboratory investigation on local scour at bridge abutments in cohesive soils are presented. Kaolin clay was used as a bed material and vertical wall abutments with three different sizes. Forty experiments were conducted under clear-water conditions in cohesive soil with a clay content ranging from 2 to 20%, compaction ranges from 57 to 88%, liquidity index ranges from 0.03 to 0.99 and the approach flow Froude numbers from 0.3 to 0.55. Equations were developed to predict the equilibrium scour pattern around the vertical bridge abutment, including the maximum scour depth, scour volume, scour width, lateral side slope, and longitudinal slopes of the scour hole, in terms of the dominating factors controlling the scour process, namely the Froude number, clay content, compaction, water content, liquid limit, plastic limit, and vertical-wall abutments dimensions. Also, an equation was developed to predict the development of scour depth with time. Comparisons with previous results are also discussed.

Keywords: Bridge abutment; cohesive soil; experimentation; open channel flow; scour

1 Introduction

Local scour at bridge abutments in cohesive soils was investigated during the past years and the scour mechanism was described (Shen *et al.* 1969, Breusers *et al.* 1977, Melville and Sutherland 1988, Molinas *et al.* 1998, Briaud *et al.* 1999, Ting *et al.* 2001, Mostafa 2003). Most of the studies focused on the equilibrium scour depth in sandy soils. Formulas are available to estimate the equilibrium scour depth at bridge abutments (e.g. Froehlich 1989, Melville 1992, Lim 1997). However, few investigations are available for determining the equilibrium scour hole in cohesive soils (e.g. Yakoub 1995, Molinas *et al.* 1998, Imran and Miah 2004) because these do not consider the individual effects of the Froude number, clay content, compaction, liquidity index, or abutment dimensions.

The scour mechanisms and dominating factors are different for cohesive and non-cohesive soils. In the latter, particle size and the submerged weight control the process so that they are used to express scour threshold and inception (e.g. Shields' and Hjulstrom's curves). The scour process of cohesive soil cannot be characterized by the particle size (Mirtskhoulava 1991). Cohesive soils consist primarily of fine-grained particles that exhibit cohesive properties which coalesce the individual particles to form a soil mass. Cohesion forces between the fine-grained particles dominate the physical and chemical particle properties as well as the properties of organic soil material. Also, the chemical properties of the pore water affects cohesion. Inception of scour occurs if the erosive forces generated by the water flow overcome the cohesion forces between the soil particles (Kuti and Yen 1976, Mirtskhoulava 1991, Annandale 1995, Kessel and Blom 1998).

Revision received 16 December 2011/Open for discussion until 31 October 2012.

ISSN 0022-1686 print/ISSN 1814-2079 online
http://www.tandfonline.com

The cohesion properties of soil are attributed mainly to clay mineralogy, clay content, compaction, and the liquidity index. Clay mineralogy characterized by a layered structure usually consists of two sheets: silicon–oxygen sheet and a cation sheet. The clay type C_t depends on the kind of cations. The most common clay types are kaolinite, montmorillonite, illite, chlorite, and bentonite. There are several common varieties of clays, as they usually exist in nature mixed together and also contain sand and silt (Graf 1984, Mirtskhoulava 1988, Raudkivi 1990).

The clay content C_c is defined as the clay percentage in the soil mixture. Increasing it increases cohesion and erosion resistance but decreases the erosion rate (Hosny 1995).

Compaction C_{omp} is defined as the percentage of the dry soil density with respect to its optimum dry density obtained from a Proctor test. Lyle and Smerdon (1965) found an increase in resistance with increasing compaction and density associated with compaction.

The water content W_c is defined as the percentage of moisture in the soil, based on the weight. Mostafa (2003) stated that water is the main agent generating cohesion forces between clay particles of cohesive soil. When the water content is less, there is not enough water to redistribute the cations and anions on the clay particle surfaces. Therefore, small van der Waals forces exist in the soil. By increasing the water content, more cations and anions on the clay particles are redistributed on the particle surfaces resulting in higher van der Waals forces and, therefore, cohesion increases until it reaches its maximum around the optimum water content. Therefore, resistance is expected to be maximum at the optimum condition. Increasing water content above the optimum condition increases the distance between the clay particles, so that the cohesion forces decrease. In addition, water starts to act as a lubricant that facilitates clay particles slipping on each other. At very large water content, clay acts as a slurry and flows as a fluid.

Consistency or plasticity of a cohesive soil depends on the water content. Atterberg defines the limits of consistency, the liquid limit W_{LL} and the plastic limit W_{PL}. The liquid limit is defined as the moisture content by weight at which the soil starts to flow if jarred slightly. The plastic limit is the lowest moisture content by weight at which the soil is still cohesive. The plasticity index, PI, is the range of moisture content between the liquid and plastic limits representing the range in which the soil is plastic. Resistance indicates an increase with the plasticity index (Graf 1984, after Grim 1962).

The liquidity index, LI, describes the ratio between the excess water content of the soil above the plastic limit and the range in which the soil is plastic. Locat and Demers (1988) found a decrease of the scour resistance as the liquidity index in the plastic regime increases.

The present study aims to obtain the scour pattern at vertical bridge abutments in a clayey soil, to develop a set of equations for equilibrium scour patterns, depth, width, volume, transverse side slope, and longitudinal slope of the scour hole in terms of the main factors including the Froude number, compaction, clay content, liquidity index, and the abutment dimensions.

2 Laboratory investigations

Experiments were conducted at a laboratory flume of the hydraulic laboratory of Cairo University, Egypt. The flume is 7m long, 1m wide and 0.5m deep. Two pumps were used to circulate the water. The first had a discharge up to $Q = 0.050\text{m}^3/\text{s}$, whereas the capacity of the second was $0.030\text{m}^3/\text{s}$. Both pumps fed the flume separately or together. The flow passed an intake gravel tank and a screen to reduce turbulence at the flume entrance. A wooden floating plate absorbed the generated surface waves. The test section was about 1.40m long. A calibrated flow meter, fitted at the flume inlet, was used to measure a discharge within ±5.0%. The flow depth was adjusted by a tailgate. A point gauge of ±0.1mm reading accuracy was used to measure the flow depths.

The experiments were conducted with flow depths d_w ranging from 10 to 14cm and the approach flow Froude number $\mathsf{F} = U/(gy)^{1/2}$ ranged from 0.30 to 0.55. Three vertical steel abutments were used in which protrusion length, L, was 7.5, 10, and 15cm and the streamwise abutment length, a, was 15, 20, and 30cm, respectively, resulting in a similar ratio of abutment to protrusion lengths. A scour test started with a selected flow depth and discharge. It lasted until equilibrium scour was attained, i.e. an increase in maximum scour depth of less than 1mm over a 24-h period (Yakoub 1995, Molinas *et al.* 1998, Mostafa 2003).

The kaolin clay used was subjected to different tests in order to determine its physical and chemical properties. Its median particle size was $D_{50} = 0.13\mu\text{m}$ and pH values ranged from 4.0 to 4.5. Other properties were: $W_{LL} = 46.6\%$, $W_{PL} = 21.4\%$, $\text{PI} = 25.2\%$, optimum water content $W_{op} = 21\%$, and moisture of natural clay of 0.6%. The kaolin clay used contained 55% silicon dioxide, 33% aluminium oxide, 0.75% iron oxide, 1.7% titanium dioxide, 0.115% potassium oxide, 0.8% sodium oxide, 0.2% magnesium oxide, and 0.075% calcium oxide. Crushed silica of $D_{50} = 4.4\mu\text{m}$ and $\text{pH} = 7.0$ was used in the soil mixture. The crystalline silica for laboratory tests was quartz-based.

The soil mixture contained crushed silica and kaolin clay. The silica was a fine-grained material and the kaolin clay was added to the mixture to provide cohesion. The soils used herein were subjected to standard geotechnical tests in order to determine their properties. The grain size distribution was determined using the hydrometer test. The standard water content test was performed to determine the water content, W_c, of the cohesive soil. The liquid and plastic limit tests were performed to determine PI and LI. The standard compaction test (Proctor test) was carried out to determine the relationship between dry-unit weight ρ_d and the water content W_c. From this, W_{op} and the related maximum soil density were determined. All geotechnical tests were performed according to ASTM (American Society for Testing

Table 1 Clay content, liquid limit, plastic limit, and plasticity index for various silica and kaolin clay mixtures

C_c (%)	W_{LL} (%)	W_{PL} (%)	PI (%)
0	–	–	–
2	28.8	17.8	11
5	30.4	18.0	12.4
10	33.1	18.7	14.4
20	36.6	19.5	17.1
30	38.5	20.2	18.3

and Materials) and AASHTO (American Association of State Highway and Transportation Office) standards.

Various mixtures of around 100g with different percentages of kaolin clay $C_c = 0, 2, 5, 10, 20$, and 30% were prepared. For each, the water content based on weight was increased gradually from 14 to 48%. Their texture and resistance for each clay and water content were investigated visually and 'friction by hand'. Then, the W_{LL} and P_{LL} tests were made (Table 1). The values indicate that: (1) cohesion is not present for the silica of any water content without kaolin clay, (1) for the percentages of kaolin clay used, cohesion effects start at $W_c = 17.8\%$, (3) for the kaolin clay, the mixture starts to act as slurry and flows as a fluid, if $W_c \geq 28.8\%$, and (2) resistance and cohesion of the mixture increase with C_c.

The experiment consisted of 40 runs with the kaolin clay mixed with silica and varied clay contents, compactions, and liquidity indices. In the first test series, the effect of clay content was investigated by varying the percentage of clay from 2, 5, 10 to 20%. The indices considered were $C_c = 69\%$ and PI = 0.25, respectively (Table 2).

In the second test series, mixture compaction was varied, including 57, 69, 80, and 88%. The clay content and liquidity indices were kept almost constant for two cases, namely at $C_c = 5\%$ and LI = 0.25, and at 20% and 0.65 (Tables 3 and 4).

For the third test series, the liquidity index varied from 0.03, 0.25, 0.65 to 0.99 thereby keeping constant $C_c = 5\%$ and $C_{omp} = 80\%$, and $C_c = 20\%$ and $C_{omp} = 69\%$ (Tables 5 and 6; Elzahry 2009).

3 Analysis of experiments

3.1 *Equilibrium scour depth*

The equilibrium scour depth d_{sec} decreased as C_c increased from 2 to 10% for all Froude numbers F. Increasing C_c further to 20% indicates a small reduction of d_{sec} because of the increased cohesion (Fig. 1).

Table 2 Summary of runs including effect of clay content on equilibrium scour geometry for $C_c = 69\%$ and LI = 0.25

Run (–)	Q (m^3/s)	C_c (%)	C_{omp} (%)	W_c (%)	LI (–)	L (m)	d_w (m)	U (m/s)	F (–)	d_{sec} (m)	V_{sec} (m^3)	t_e (h)
KC-10-1	0.0384	20	70.9	23.84	0.24	0.100	0.120	0.32	0.30	0.013	0.00004	72
KC-10-2	0.0475	20	71.2	24.11	0.26	0.100	0.119	0.40	0.37	0.027	0.00022	66
KC-10-3	0.0613	20	69.4	23.75	0.24	0.100	0.122	0.50	0.46	0.047	0.00036	60
KC-10-4	0.0704	20	70.5	23.68	0.23	0.100	0.119	0.59	0.55	0.062	0.00123	54
KC-10-5	0.0387	10	68.5	21.98	0.23	0.100	0.120	0.32	0.30	0.026	0.00013	66
KC-10-6	0.0480	10	69.8	22.39	0.26	0.100	0.120	0.40	0.37	0.049	0.00047	60
KC-10-7	0.0609	10	69.9	22.33	0.25	0.100	0.121	0.50	0.46	0.068	0.00110	54
KC-10-8	0.0702	10	67.2	22.18	0.24	0.100	0.119	0.59	0.55	0.090	0.00228	48
KC-10-9	0.0345	5	67.7	20.98	0.24	0.100	0.110	0.31	0.30	0.038	0.00050	60
KC-10-10	0.0481	5	68.5	20.87	0.23	0.100	0.120	0.40	0.37	0.070	0.00204	54
KC-10-11	0.0619	5	69.6	20.79	0.23	0.100	0.123	0.50	0.46	0.094	0.00307	48
KC-10-12	0.0626	5	68.9	20.95	0.24	0.100	0.110	0.57	0.55	0.108	0.00341	42
KC-10-13	0.0386	2	66.8	20.55	0.25	0.100	0.120	0.32	0.30	0.046	0.00075	54
KC-10-14	0.0478	2	68.3	20.62	0.26	0.100	0.120	0.40	0.37	0.084	0.00283	48
KC-10-15	0.0616	2	67.9	20.46	0.24	0.100	0.122	0.50	0.46	0.114	0.00555	42
KC-10-16	0.0706	2	67.2	20.32	0.23	0.100	0.119	0.59	0.55	0.140	0.00872	36

Table 3 Summary of runs representing effect of compaction on equilibrium scour geometry for $C_c = 5\%$ and LI = 0.25

Run (–)	Q (m^3/s)	C_c (%)	C_{omp} (%)	W_c (%)	LI (–)	L (m)	d_w (m)	U (m/s)	F (–)	d_{sec} (m)	V_{sec} (m^3)	t_e (h)
KC-10-17	0.0456	5	88.4	21.22	0.26	0.100	0.134	0.34	0.30	0.017	0.00006	72
KC-10-18	0.0468	5	88.1	20.93	0.24	0.100	0.102	0.46	0.46	0.043	0.00045	60
KC-15-19	0.0483	5	79.8	20.88	0.23	0.150	0.139	0.35	0.30	0.041	0.00081	66
KC-15-20	0.0574	5	78.9	21.06	0.25	0.150	0.117	0.49	0.46	0.083	0.00499	54
KC-10-9	0.0345	5	67.7	20.98	0.24	0.100	0.110	0.31	0.30	0.038	0.00050	60
KC-10-11	0.0619	5	69.6	20.79	0.23	0.100	0.123	0.50	0.46	0.070	0.00204	48
KC-10-21	0.0418	5	57.7	21.14	0.25	0.100	0.126	0.33	0.30	0.057	0.00074	54
KC-10-22	0.0584	5	57.1	20.89	0.23	0.100	0.118	0.49	0.46	0.148	0.00834	42

Table 4 Summary of runs representing effect of compaction on equilibrium scour geometry for $C_c = 20\%$ and LI = 0.65

Run (–)	Q (m^3/s)	C_c (%)	C_{omp} (%)	W_c (%)	LI (–)	L (m)	d_w (m)	U (m/s)	F (–)	d_{sec} (m)	V_{sec} (m^3)	t_e (h)
KC-10-23	0.0442	20	89.0	30.71	0.65	0.100	0.113	0.39	0.37	0.024	0.00012	72
KC-10-24	0.0601	20	89.3	30.78	0.65	0.100	0.107	0.56	0.55	0.042	0.00043	60
KC-10-25	0.0486	20	80.2	31.10	0.67	0.100	0.121	0.40	0.37	0.036	0.00029	66
KC-10-26	0.0684	20	79.4	31.04	0.67	0.100	0.116	0.59	0.55	0.064	0.00180	54
KC-7.5-27	0.0586	20	69.5	30.86	0.66	0.075	0.137	0.43	0.37	0.041	0.00032	60
KC-7.5-28	0.0693	20	69.3	30.77	0.65	0.075	0.117	0.59	0.55	0.077	0.00272	48
KC-10-29	0.0470	20	58.0	30.82	0.66	0.100	0.118	0.40	0.37	0.066	0.00218	54
KC-10-30	0.0580	20	57.6	30.46	0.63	0.100	0.104	0.56	0.55	0.158	0.01138	42

Table 5 Summary of runs representing effect of liquidity index on equilibrium scour geometry for $C_c = 5\%$ and $C_{omp} = 80\%$

Run (–)	Q (m^3/s)	C_c (%)	C_{omp} (%)	W_c (%)	LI (–)	L (m)	d_w (m)	U (m/s)	F (–)	d_{sec} (m)	V_{sec} (m^3)	t_e (h)
KC-10-31	0.0403	5	76.7	30.32	0.99	0.100	0.123	0.33	0.30	0.075	0.00153	54
KC-10-32	0.0480	5	76.9	30.26	0.99	0.100	0.104	0.46	0.46	0.142	0.01004	42
KC-7.5-33	0.0396	5	78.5	26.13	0.66	0.075	0.122	0.32	0.30	0.042	0.00030	60
KC-7.5-34	0.0500	5	78.2	26.28	0.67	0.075	0.107	0.47	0.46	0.082	0.00189	48
KC-15-19	0.0483	5	79.8	20.88	0.23	0.150	0.139	0.35	0.30	0.041	0.00081	66
KC-15-20	0.0574	5	78.9	21.06	0.25	0.150	0.117	0.49	0.46	0.083	0.00499	54
KC-10-35	0.0378	5	78.3	18.30	0.02	0.100	0.118	0.32	0.30	0.018	0.00007	72
KC-10-36	0.0614	5	78.6	18.45	0.04	0.100	0.122	0.50	0.46	0.060	0.00094	60

Table 6 Summary of runs representing effect of liquidity index on equilibrium scour geometry for $C_c = 20\%$ and $C_{omp} = 69\%$

Run (–)	Q (m^3/s)	C_c (%)	C_{omp} (%)	W_c (%)	LI (–)	L (m)	d_w (m)	U (m/s)	F (–)	d_{sec} (m)	V_{sec} (m^3)	t_e (h)
KC-10-37	0.0486	20	67.6	36.41	0.99	0.100	0.120	0.41	0.37	0.084	0.00414	54
KC-10-38	0.0560	20	66.4	36.39	0.99	0.100	0.102	0.55	0.55	0.153	0.01142	42
KC-7.5-27	0.0586	20	69.5	30.86	0.66	0.075	0.137	0.43	0.37	0.041	0.00032	60
KC-7.5-28	0.0693	20	69.3	30.77	0.65	0.075	0.117	0.59	0.55	0.077	0.00272	48
KC-10-2	0.0475	20	71.2	24.11	0.26	0.10	0.119	0.40	0.37	0.027	0.00022	66
KC-10-4	0.0704	20	70.5	23.68	0.23	0.10	0.119	0.59	0.55	0.062	0.00123	54
KC-15-39	0.0599	20	70.1	20.08	0.02	0.150	0.140	0.43	0.37	0.031	0.00037	72
KC-15-40	0.0720	20	69.8	20.36	0.03	0.150	0.121	0.60	0.55	0.061	0.00246	60

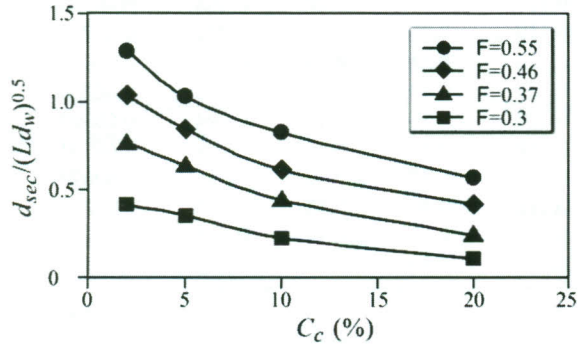

Figure 1 Variation of relative equilibrium scour depth with C_c for $C_{omp} = 0.69$ and LI = 0.25.

The relative equilibrium scour depth decreased as the percentage of mixture compaction increased from $C_{omp} = 57$ to 70% for all F. Increasing C_{omp} further to 88% has a less effect on d_{sec} because of the increase in cohesion forces (Fig. 2).

The equilibrium scour depth increased as the mixture liquidity index increased from 0.03 to 0.65 for all F. Increasing the liquidity index further from 0.65 to 0.99 has a large effect on d_{sec} (Fig. 3). For constant clay content, compaction, and liquidity indices, d_{sec} is increased with F.

3.2 *Development of scour hole with time*

At the initial scour phase, the strength of the primary vortex generated at the upstream abutment face was strong, resulting in a high erosion rate. As the scour hole deepens, the primary vortex becomes weaker, so that the rates of applied shear stress and that of scour decrease until reaching the equilibrium condition. This condition was reached asymptotically for clear-water scour. The slope of the curve scour depth versus time t gives the scour rate. Figure 4 shows the dimensionless temporal depth variation $(d_{sc(t)}/d_{sec})[t/t_e]$ at the upstream wall abutment, normalized by d_{sec} for the considered test. Time t was normalized by the time to reach the equilibrium scour t_e in this test. For a given F, the scour rate increased more for tests of low clay content, low compaction, and high liquidity index than otherwise.

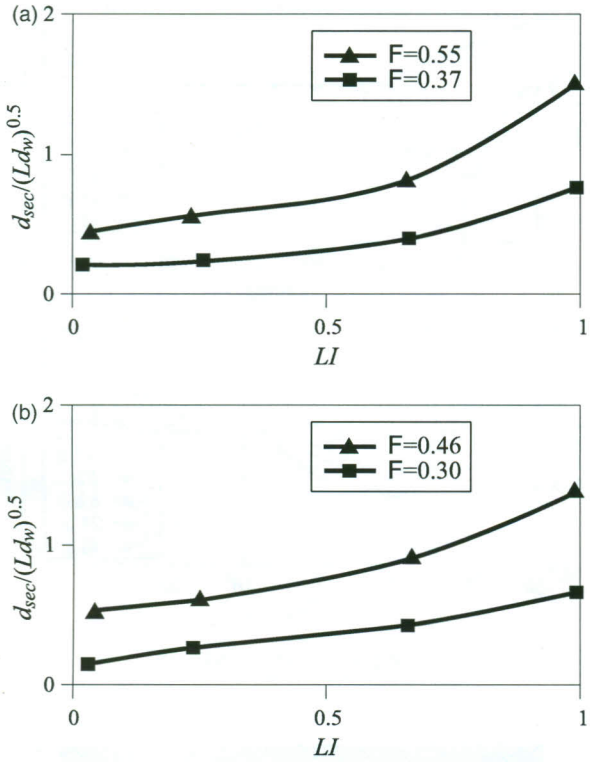

Figure 2 Variation of relative equilibrium scour depth with C_{omp} for: (a) $C_c = 0.20$, LI = 0.65 and (b) $C_c = 0.05$, LI = 0.25.

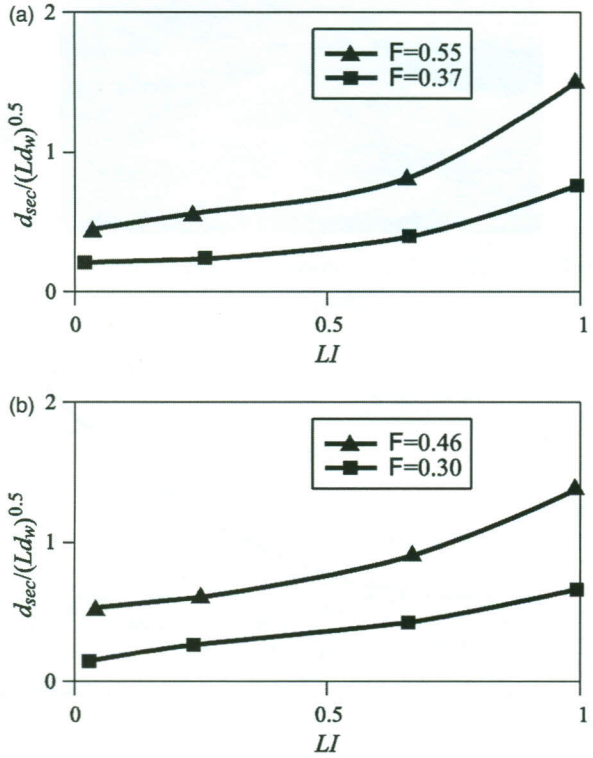

Figure 3 Variation of relative equilibrium scour depth with LI for: (a) $C_c = 0.20$, $C_{omp} = 0.69$ and (b) $C_c = 0.05$, $C_{omp} = 0.80$.

Figure 5 shows the temporal advance of the scour hole and Fig. 6 shows the lateral and longitudinal profiles of the scour hole for run KC-10-11 with $C_c = 5\%$, $C_{omp} = 70\%$, LI = 0.25,

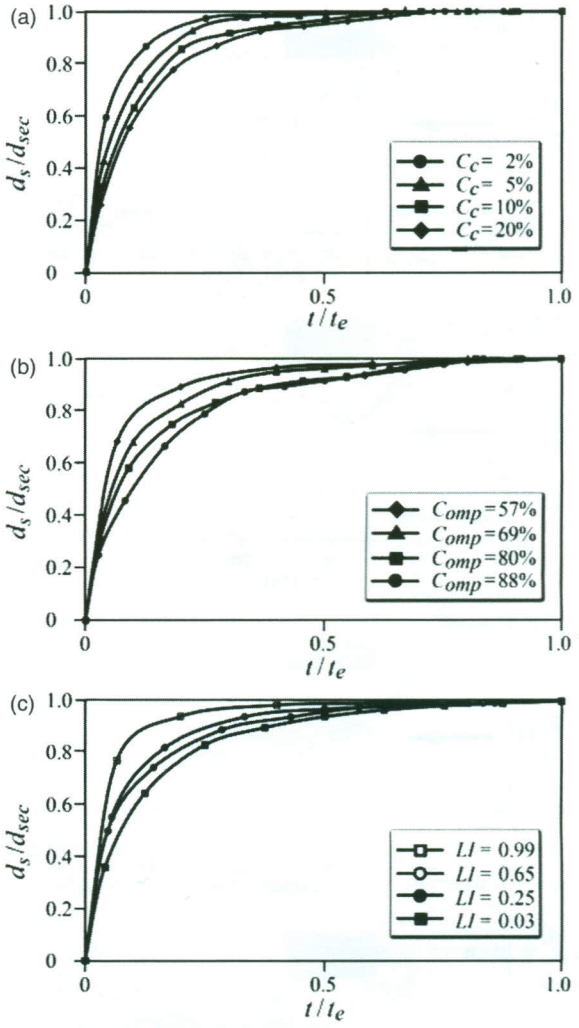

Figure 4 Temporal development of relative scour depth for (a) $C_{omp} = 0.69$, LI = 0.25, F = 0.37, (b) $C_c = 0.20$, LI = 0.65, F = 0.37, (c) $C_c = 0.05$, $C_{omp} = 0.80$, F = 0.46.

and F = 0.46 after t = 0.5, 2, 6, 24, and 48h. Scour initiates at the upstream nose of the vertical wall abutment and progresses downstream. The horizontal limits of the scour hole in the longitudinal direction x and the lateral direction y increase with scour advance until reaching equilibrium. The rate of increase reduced with time. The lateral side slope of the scour hole also decreased during scour hole development.

3.3 *Scour hole geometry*

Figure 7 shows a typical equilibrium scour pattern. The scour hole at the upstream abutment nose has the shape of a partial inverted cone with a rippled surface. Its deepest point is located at the upstream nose where the slope of the scour hole is steep. This slope reduces near the downstream abutment end. In cohesive scour processes, once the sediment particles are scoured from the alluvial bottom, they remain in suspension and are transported in the downstream direction without deposition up- or downstream from the scour hole. The dimensionless equilibrium scour volume V_{sec}/L^3 increases with d_{sec}/L (Fig. 8).

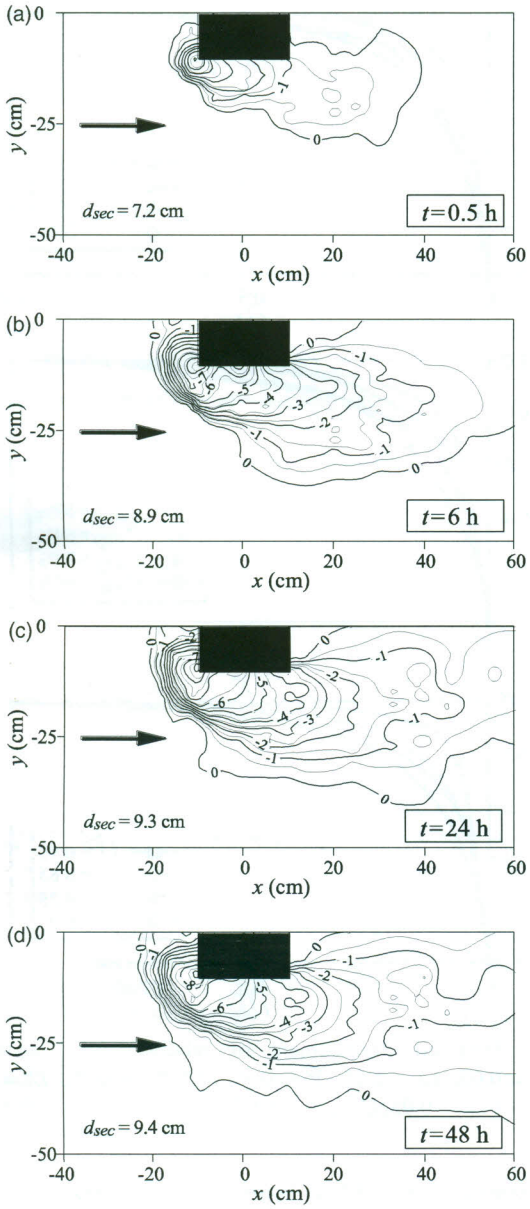

Figure 5 Temporal development of depth contour of scour hole for Run KC-10-11 at t = (*a*) 0.5 h, (b) 6 h, (c) 24 h, and (d) 48 h.

3.4 *Equilibrium scour width*

The equilibrium scour hole width w_{sec} was measured from the upstream abutment nose perpendicular to the approach flow. The equilibrium scour width increases with the equilibrium scour depth (Fig. 9).

3.5 *Lateral profile of scour hole*

The lateral scour hole profile is a section perpendicular to the approach flow direction at the upstream abutment face. Its equilibrium lateral side slope is inversely proportional to F and LI, and proportional to C_c and C_{omp}. As C_c increases from 2 to 20%, d_{sec} reduced by 29% for F = 0.3, whereas for F = 0.55, d_{sec} decreased by 46% (Fig. 10a).

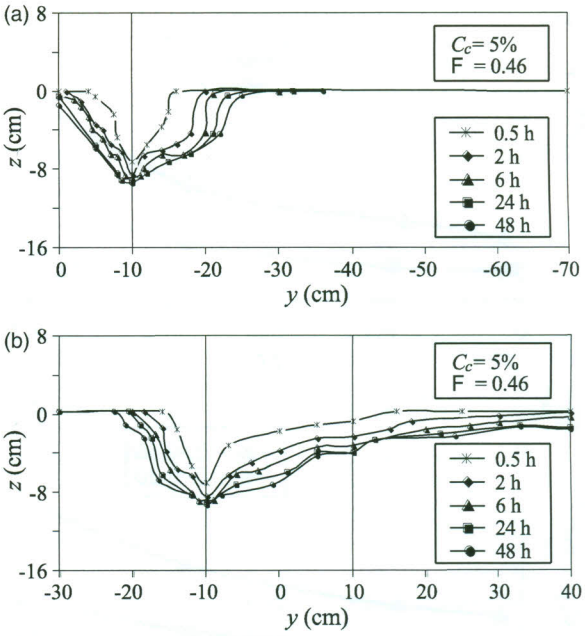

Figure 6 Temporal scour profiles for test KC-10-11.

Figure 7 Eroded clay bed, no downstream deposition

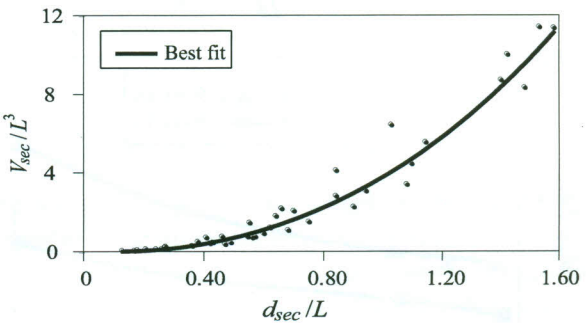

Figure 8 Variation of relative scour volume with equilibrium scour depth

As C_{omp} increases from 57 to 88%, d_{sec} decreased by 36% for F = 0.37, whereas for F = 0.55, d_{sec} decreases by 27% (Fig. 10b). As LI decreased from 0.99 to 0.03, d_{sec} decreased by 25% for F = 0.3, whereas for F = 0.46, d_{sec} decreased by 42% (Fig. 10c).

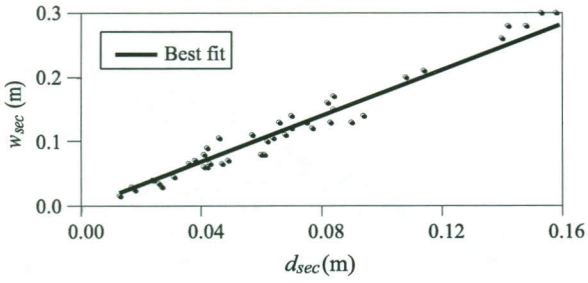

Figure 9 Variation of equilibrium scour width with scour depth

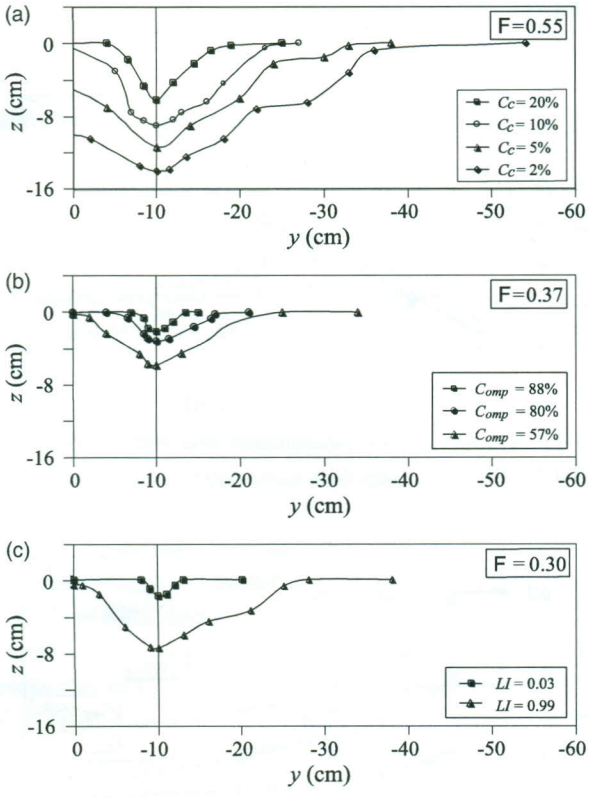

Figure 10 Variation of scour hole profile in a lateral direction (a) $C_{omp} = 0.69$, LI = 0.25, (b) $C_c = 0.20$, LI = 0.65 and (c) $C_c = 0.05$, $C_{omp} = 0.80$.

3.6 *Longitudinal scour hole profile*

For each soil mixture, the scour hole has a certain slope along the streamwise flow direction. As shown in Fig. 11, the equilibrium upstream slope of the scour hole is two to four times steeper than that of the downstream. Both the up- and downstream equilibrium slopes are inversely proportional to F and LI, and proportional to the clay content and compaction.

4 Dimensional analyses for clay

The depth of scour d_{sec} may be expressed as

$$d_{sec} = f(\Delta S, C_t, C_c, C_{omp}, D_{50}, W_c, W_{LL}, W_{PL}, g, \rho, m, d_w, U, L, a, K_s, K_q, B, t_e) \quad (1)$$

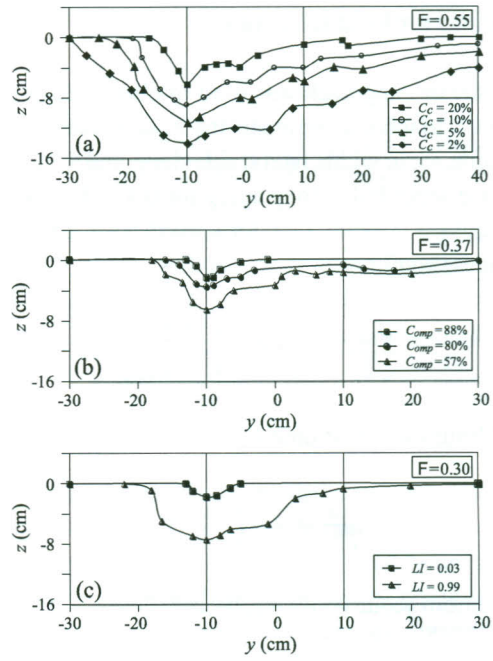

Figure 11 Variation of scour hole profile in a longitudinal direction (a) $C_{omp} = 0.69$, LI = 0.025, (b) $C_c = 0.20$, LI = 0.65, and (c) $C_c = 0.05$, $C_{omp} = 0.80$.

The chemical properties of cohesive soil can be lumped into the salinity difference ΔS between the flowing and the pore water. The physical and mechanical properties of cohesive soil are represented by C_t, C_c, C_{omp}, D_{50}, W_c, W_{LL}, and W_{PL}. The physical and chemical flow properties are represented by ρ, μ, g, y, and U, where ρ is the water density, μ the dynamic water viscosity, g the gravity acceleration, y the average approach flow depth, and U the approach flow velocity. The abutment and flume properties are represented by L, a, K_s, K_θ, and B, where K_s is the abutment shape factor, K_θ the abutment alignment factor, and B the flume width. The quantities W_c, W_{LL}, and W_{PL} are combined with the non-dimensional liquidity index

$$LI = \frac{W_c - W_{PL}}{W_{LL} - W_{PL}} \quad (2)$$

Equation (1) then reduces to

$$d_{sec} = f(C_c, C_{omp}, \mathrm{LI}, g, \rho, m, y, U, L, a, t_e) \quad (3)$$

Using the π-theorem, $\mathsf{F} = [U/(gy)^{1/2}]$ as the Froude number and $\mathsf{R} = [(\rho g^{1/2} y^{3/2})/\mu]$ as the Reynolds number, then

$$\frac{d_{sec}}{\sqrt{Ly}} = \left(C_c, C_{omp}, LI, \frac{a}{L}, \mathsf{F}, \mathsf{R}, \frac{Ut_e}{y}\right) \quad (4)$$

For fully-turbulent open channel flow and constant a/L, the effect of R is negligible, so that Eq. (4) is written as

$$\frac{d_{sec}}{\sqrt{Ly}} = \left(C_c, C_{omp}, LI, \mathsf{F}, \frac{Ut_e}{y}\right) \quad (5)$$

5 Equations for local scour in clay

The least squares approach was used to obtain relations among the various variables to estimate the equilibrium scour depth, scour volume, scour width, lateral side slope, and the longitudinal slopes of the scour hole. They apply for $0.3 \leq \mathsf{F} \leq 0.55$, $2\% \leq C_c(\%) \leq 20\%$, $57\% \leq C_{omp} \leq 88\%$, and $0.03 \leq \mathrm{LI} \leq 0.99$. The dimensionless equilibrium scour depth is

$$\frac{d_{sec}}{\sqrt{Ly}} = 209530 \frac{\mathsf{F}^{1.68} LI^{0.48}}{C_c^{0.35} C_{omp}^{2.36}} \tag{6}$$

The equilibrium scour volume V_{sec} is

$$\frac{V_{sec}}{L^3} = 4.0 \left(\frac{d_{sec}}{L}\right)^{2.3} \tag{7}$$

The equilibrium scour width w_{sec} is as follows:

$$w_{sec} = 1.8 d_{sec} \tag{8}$$

The lateral side angle of the scour hole θ_{side} (in deg.) is

$$\theta_{side} = 0.74\ \mathsf{F}^{-0.03} C_c^{0.09} C_{omp}^{0.79} LI^{-0.10} \tag{9}$$

The longitudinal upstream angle θ_{up} (in deg.) is

$$\theta_{up} = 2.53\ \mathsf{F}^{-0.02} C_c^{0.07} C_{omp}^{0.59} LI^{-0.06} \tag{10}$$

The longitudinal downstream angle θ_{down} (in deg.) is

$$\theta_{down} = 0.009\ \mathsf{F}^{-1.08} C_c^{0.17} C_{omp}^{1.35} LI^{-0.13} \tag{11}$$

The equilibrium time of scour t_e (in hour) is

$$\frac{Ut_e}{y} = 27000\ \mathsf{F}^{0.58} C_c^{0.12} C_{omp}^{0.82} LI^{-0.05} \tag{12}$$

The development of a non-dimensional scour depth with time finally is as follows:

$$\frac{d_{sc(t)}}{d_{sec}} = \left(\frac{t}{t_e}\right)^{0.158} \tag{13}$$

6 Comparison with previous studies

Figure 12 compares the equilibrium scour depths computed using Eq. (4) with the measured data. Some 82% of the latter are within ±20%, indicating a reasonable prediction of d_{sec}.

Figure 13 compares the equilibrium scour times computed from Eq. (10) with the measured data. Some 87% of the latter are within ±10%, indicating again a reasonable prediction of t_e.

Yakoub (1995) and Molinas *et al.* (1998) used the kaolin clay for clear-water scour at bridge abutments, deriving equations to estimate the equilibrium scour depth. The clay content of Yakoub ranged from 0 to 30%, and from 0 to 11% by Molinas. Herein, it ranged from 2 to 20%. Compaction and liquidity indices had no effect on the Yakoub and Molinas scour depth equations, whereas the present study indicates that these are major parameters. Figure 14 compares d_{sec} computed from Eq. (4) with the results of Yakoub (1995) and Molinas *et al.* (1998) for $\mathsf{F} = 0.4$ and $\mathrm{LI} = 0.25$.

The equilibrium scour depth computed by Yakoub (1995) is similar to that given herein for $C_{omp} = 60\%$ and $2\% \leq C_c \leq 6\%$ or for $C_{omp} = 70\%$ and $6\% \leq C_c \leq 15\%$. His equation has the same trend as that of the present. Note that compactions and

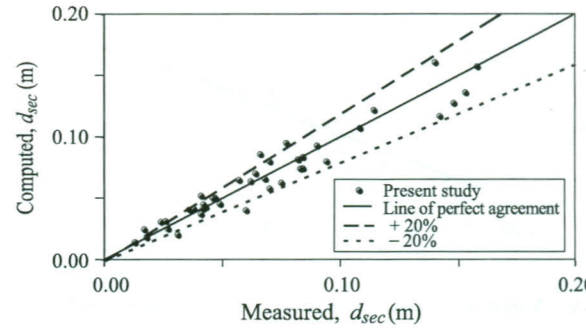

Figure 12 Comparison of experimental data with results obtained using Eq. (4).

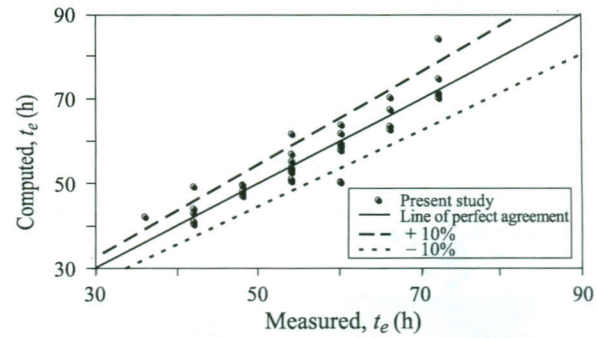

Figure 13 Comparison of experimental data with results obtained using Eq. (10).

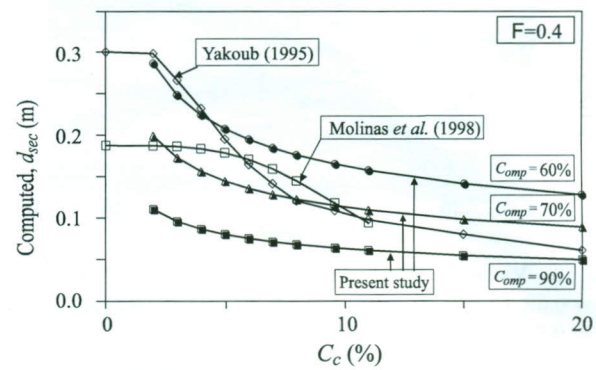

Figure 14 Comparison of results obtained by Eq. (4) with these of Yakoub (1995) and Molinas *et al.* (1998)

Table 7 Yakoub's (1995) kaolin clay tests for F = 0.4

C_c (%)	0	10	20	30
C_{omp} (%)	91	86	86	85
W_c (%)	4	13	16	22

Table 8 Molina's (1998) kaolin clay tests for F = 0.4

C_c (%)	0	5	10	13
C_{omp} (%)	91	70	70	63
W_c (%)	4	6.9	11.4	11

liquidity indices are not constants as reported by Yakoub (1995) (Table 7).

The equilibrium scour depth computed by Molinas *et al.* (1998) is similar to that given herein for $C_{omp} = 70\%$ and $2\% \leq C_c \leq 3\%$ or from 10 to 11%. Between $3\% \leq C_c \leq 10\%$, the trend of his equation differs from that of the present, which is attributed to the variability of the compaction and liquidity indices (Table 8).

7 Comparison between sand and clay

Herein, the kaolin clay content ranged from 2 to 20%, compaction from 57 to 88%, and LI from 0.03 to 0.99. Clay of 20% clay content, $C_{omp} = 88\%$, and LI = 0.03 result in small scour. Clay of $C_c = 10\%$, $C_{omp} = 72\%$, and LI = 0.50 result in medium scour, whereas clay of $C_c = 2\%$, $C_{omp} = 57\%$, and of LI = 0.99 result in high scour. Figure 15 compares the equilibrium scour depths in a sandy soil for $D_{50} = 0.38$ mm from Froehlich (1989) and the equilibrium scour depth in kaolinite clay. The comparison range of F is below 0.25 to satisfy the clear-water scour condition.

For F = 0.25, the ratio of equilibrium scour depths for the sandy soil and the kaolin clay is shown in Table 9, indicating that the common practice used to estimate the local scour depth soil by scour formulas developed for sandy soil is invalid.

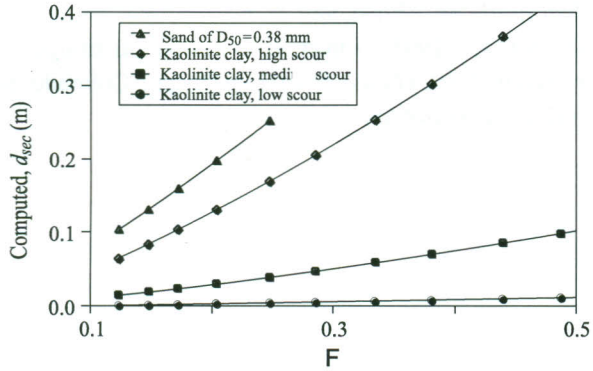

Figure 15 Comparison of equilibrium scour depth for a sandy soil and clay.

Table 9 Ratios of equilibrium scour depth for sandy soil to kaolin clay

	F = 0.25		
	Low scour $C_c = 20\%$, $C_{omp} = 88\%$, LI = 0.03	Medium scour $C_c = 10\%$, $C_{omp} = 72\%$, LI = 0.50	High scour $C_c = 2\%$, $C_{omp} = 57\%$, LI = 0.99
$\frac{d_{sec}\text{ (sand)}}{d_{sec}\text{ (kaolinite clay)}}$	50	6.5	1.5

8 Conclusions

The scour patterns at bridge abutments in a clayey soil are mainly affected by the approach flow Froude number, the clay content, compaction, and the liquidity index. The equilibrium scour depth is proportional to the Froude number and the liquidity index but inversely proportional to the clay content and compaction.

As the clay content increases from 2 to 20%, the equilibrium scour depth decreases by 29% for an approach flow Froude number of 0.3, whereas for 0.55, the equilibrium scour depth decreases by 46%. As the soil compaction increases from 57 to 88%, the equilibrium scour depth decreases by 36% for an approach flow Froude number of 0.37, and by 27% for an approach flow Froude number of 0.55. As the liquidity index decreases from 0.99 to 0.03, the equilibrium scour depth decreases by 25% for an approach flow Froude number of 0.3 and by 42% for an approach flow Froude number of 0.46.

The equilibrium scour width is approximately 1.8 times the equilibrium scour depth. Practical formulas are developed to predict the equilibrium scour pattern, including the equilibrium scour depth, width, volume, and side and longitudinal slopes of the scour hole around a bridge abutment in terms of the approach flow Froude number, the clay content, compaction, liquidity index, and abutment dimensions. The ratios of equilibrium scour depth for a sandy soil to that for a kaolin clay of low, medium, and high scour potential are 50, 6.5, and 1.5, respectively.

Notation

a = streamwise abutment length (m)
B = flume width (m)
C_c = clay content (–)
C_{omp} = compaction degree related to optimum value (–)
D_{50} = median sediment size (m)
$d_{sc(t)}$ = scour depth in cohesive soil (m)
d_{sec} = equilibrium scour depth (m)
F = approach flow Froude number $(U/(gy)^{1/2})$ (–)
g = gravitational acceleration (m/s^2)
K_θ = abutment alignment factor (–)
K_s = abutment shape factor (–)
L = abutment width (m)

LI = liquidity index (–)
PI = plasticity index (–)
R = Reynolds number (–)
t_e = equilibrium time of scour (h)
U = approach flow velocity (m/s)
V_{sec} = equilibrium scour volume (m^3)
W_c = water content based on weight (–)
W_{LL} = liquid limit of cohesive soil (–)
W_{PL} = plasticity limit of cohesive soil (–)
w_{sec} = equilibrium scour width (m)
y = approach flow depth (m)
ΔS = salinity difference between water flow and pore water (ppm)
θ_{down} = downstream longitudinal angle (–)
θ_{side} = side angle of scour hole (–)
θ_{up} = upstream longitudinal angle (–)
μ = dynamic water viscosity (kg/sm)
ρ = density of clear water (kg/m^3)

References

Annandale, G.W. (1995). Erodibility. *J. Hydraulic Res.* 33(2), 471–494.

Breusers, H.N.C., Nicollet, G., Shen, H.W. (1977). Local scour around cylindrical piers. *J. Hydraulic Res.* 15(3), 221–252.

Briaud, J.L., Ting, F.C.K., Chen, H.C., Gudavalli, R., Perugu, S., Wei, G. (1999). SRICOS: Prediction of scour rate in cohesive soils at bridge piers. *J. Geotech. Eng.* 125(2), 237–246.

Elzahry, E.F.M. (2009). Scour at bridges abutments in cohesive soil. *PhD Thesis*. Dept. Civil Eng., Faculty of Eng., (Shobra), Benha University, Egypt.

Froehlich, D.C. (1989). *Abutment scour prediction*. Transportation Research Board, Washington DC.

Graf, W.H. (1984). *Hydraulics of sediment transport*. Water Resources Publications, Littleton CO.

Grim, R.E. (1962). *Applied clay mineralogy*. McGraw-Hill, New York.

Hosny, H.M. (1995). Experimental study of local scour around circular bridge piers in cohesive soils. *PhD Thesis*. Civil Eng. Dept., Colorado State University, Fort Collins CO.

Imran, J., Miah, A.M. (2004). Investigation of bridge abutment scour. *Research Report* R-03-UTC-Bridge Abutment-SETS-01. University of South Carolina, Columbia SC.

Kessel, T.V., Blom, C. (1998). Rheology of cohesive sediments: Comparison between a natural and an artificial mud. *J. Hydraulic Res.* 36(2), 591-612.

Kuti, E.O., Yen, C.L. (1976). Scouring of cohesive soils. *J. Hydraulic Res.* 14(3), 195–206.

Lim, S.-Y. (1997). Equilibrium clear water scour around an abutment. *J. Hydraulic Eng.* 123(3), 237–243.

Locat, J., Demers, D. (1988). Viscosity, yield stress, remolded strength, and liquidity index relationships for sensitive clays. *Canadian Geotech. J.* 25(2), 799–806.

Lyle, W.M., Smerdon, E.T. (1965). Relation of compaction and other soil properties to the erosion resistance of soils. *Trans. ASAE* 8(3), 419–422.

Melville, B.W., Sutherland, A.J. (1988). Design method for local scour at bridge piers. *J. Hydraulic Eng.* 114(8), 1210–1226.

Melville, B.W. (1992). Local scour at bridge abutments. *J. Hydraulic Eng.* 118(2), 615–631.

Molinas, A., Abdeldayem, A. (1998). Effect of clay content on bridge scour. Proc. Int. Conf. *Water Resources Eng.* 1, 280–285. ASCE: Reston VA.

Molinas, A., Hosny, H.M., Jones, S. (1998). Pier scour in Montmorillonite clay soils. Proc. Int. Conf. *Water Resources Eng.* 1, 292–297. ASCE, Reston VA.

Molinas, A., Reiad, N., Jones, S. (1998). Effect of cohesion on abutment scour. Proc. Int. Conf. *Water Resources Eng.* 1, 252–257. ASCE, Reston VA.

Mirtskhoulava, T.Y. (1988). *Basic physics and mechanics of channel erosion*. Gidrometeoizdat, Leningrad USSR.

Mirtskhoulava, T.Y. (1991). Scouring by flowing water of cohesive and noncohesive beds. *J. Hydraulic Res.* 29(3), 341–354.

Mostafa, T.M.S. (2003). Experimental modeling of local scour in cohesive soils. *PhD dissertation*. University of South Carolina, Columbia SC.

Raudkivi, A.J. (1990). *Loose boundary hydraulics*, 3rd ed. Pergamon Press, Oxford UK.

Shen, H.W., Schneider, V.R., Karaki, S. (1969). Local scour around bridge piers. *J. Hydraulics Div.* ASCE 95(HY6), 1919–1940.

Ting, F.C.K., Briaud, J.L., Chen, H.C., Gudavalli, R., Perugu, S., Wei, G. (2001). Flume tests for scour in clay at circular piers. *J. Hydraulic Eng.* 127(9), 969–978.

Yakoub, N.G.R. (1995). Effect of cohesion on bridge abutment scour. *PhD Thesis*. Civil Eng. Dept., Colorado State University, Fort Collins CO.